A&A 549, A31 (2013)
DOI: 10.1051/0004-6361/201219435

Astronomy & Astrophysics

Herschel-ATLAS: *Planck* sources in the phase 1 fields⋆

D. Herranz[1,2], J. González-Nuevo[1,3], D. L. Clements[4], M. Clemens[5], G. De Zotti[5,3], M. Lopez-Caniego[1], A. Lapi[6,3], G. Rodighiero[7], L. Danese[3], H. Fu[8], A. Cooray[8], M. Baes[9], G. J. Bendo[10], L. Bonavera[1,3], F. J. Carrera[1], H. Dole[11], S. Eales[12], R. J. Ivison[13,14], M. Jarvis[15,16], G. Lagache[11], M. Massardi[17], M. J. Michałowski[14], M. Negrello[5], E. Rigby[18], D. Scott[19], E. Valiante[12], I. Valtchanov[20], P. Van der Werf[18], R. Auld[12], S. Buttiglione[5], A. Dariush[4], L. Dunne[21], R. Hopwood[4], C. Hoyos[21], E. Ibar[13], and S. Maddox[21]

[1] Instituto de Física de Cantabria (CSIC-UC), Avda. los Castros s/n, 39005 Santander, Spain
e-mail: herranz@ifca.unican.es
[2] Astrophysics Group, Cavendish Laboratory, University of Cambridge, Cambridge CB3 0HE, UK
[3] Astrophysics Sector, SISSA, via Bonomea 265, 34136 Trieste, Italy
[4] Astrophysics Group, Imperial College, Blackett Laboratory, Prince Consort Road, London SW7 2AZ, UK
[5] INAF-Osservatorio Astronomico di Padova, Vicolo dell'Osservatorio 5, 35122 Padova, Italy
[6] Dipartimento di Fisica, Università di Roma Tor Vergata, via Ricerca Scientifica 1, 00133 Roma, Italy
[7] Dip. Astronomia, Univ. di Padova, Vicolo dell'Osservatorio 3, 35122 Padova, Italy
[8] Department of Physics and Astronomy, Frederick Reines Hall, University of California, Irvine, CA 92697–4575, USA
[9] Sterrenkundig Observatorium, Universiteit Gent, Krijgslaan 281 S9, 9000 Gent, Belgium
[10] UK ALMA Regional Centre Node, Jodrell Bank Centre for Astrophysics, School of Physics and Astronomy, University of Manchester, Oxford Road, Manchester M13 9PL, UK
[11] Institut d'Astrophysique Spatiale (IAS), Bât. 121, Université Paris-Sud 11 and CNRS (UMR 8617), 91405 Orsay, France
[12] Cardiff School of Physics and Astronomy, Cardiff University, Queens Building, The Parade, Cardiff, CF24 3AA, UK
[13] UK Astronomy Technology Centre, Royal Observatory, Blackford Hill, Edinburgh EH9 3HJ, UK
[14] SUPA⋆⋆, Institute for Astronomy, University of Edinburgh, Royal Observatory, Edinburgh, EH9 3HJ, UK
[15] Centre for Astrophysics Research, Science & Technology Research Institute, University of Hertfordshire, Hatfield, Herts, AL10 9AB, UK
[16] Physics Department, University of the Western Cape, Cape Town, 7535, South Africa
[17] INAF-Istituto di Radioastronomia, via Gobetti 101, 40129 Bologna, Italy
[18] Leiden Observatory, Leiden University, PO Box 9513, 2300 RA Leiden, The Netherlands
[19] Department of Physics & Astronomy, University of British Columbia, 6224 Agricultural Road, Vancouver, British Columbia, Canada
[20] *Herschel* Science Centre, ESAC, ESA, PO Box 78, Villanueva de la Cañada, 28691 Madrid, Spain
[21] School of Physics and Astronomy, University of Nottingham, University Park, Nottingham NG7 2RD, UK

Received 17 April 2012 / Accepted 4 October 2012

ABSTRACT

We present the results of a cross-correlation of the *Planck* Early Release Compact Source catalogue (ERCSC) with the catalogue of *Herschel*-ATLAS sources detected in the phase 1 fields, covering 134.55 deg^2. There are 28 ERCSC sources detected by *Planck* at 857 GHz in this area. As many as 16 of them are probably high Galactic latitude cirrus; 10 additional sources can be clearly identified as bright, low-z galaxies; one further source is resolved by *Herschel* as two relatively bright sources; and the last is resolved into an unusual condensation of low-flux, probably high-redshift point sources, around a strongly lensed *Herschel*-ATLAS source at $z = 3.26$. Our results demonstrate that the higher sensitivity and higher angular resolution H-ATLAS maps provide essential information for the interpretation of candidate sources extracted from *Planck* sub-mm maps.

Key words. galaxies: general – galaxies: evolution – submillimeter: galaxies – catalogs – gravitational lensing: strong

1. Introduction

During the past year, the simultaneous operation of ESA's *Herschel* (Pilbratt et al. 2010) and *Planck* (Tauber et al. 2010; Planck Collaboration 2011a) missions has given us an unprecedented opportunity to cover one of the last few observational gaps in the far-infrared and sub-millimeter regions of the electromagnetic spectrum. *Herschel* is an observatory facility that covers the 55−671 μm spectral range, with angular resolution ranging between 6 and 35 arcsec (Pilbratt et al. 2010). *Planck* is a surveyor that is observing the whole sky in nine spectral bands between 350 μm and 1 cm with angular resolution ranging from 4.23 to 32.65 arcmin. *Planck* has two frequency channels close to the *Herschel* bands: the 545 and 857 GHz (550 and 350 μm) channels of the High Frequency Instrument (HFI). In this paper we will study the cross-correlation of the *Planck* Early Release Compact Source Catalogue (ERCSC) with the phase 1 of the catalogue of the *Herschel* Astrophysical Terahertz Large Area Survey (H-ATLAS, Eales et al. 2010).

The overlap in time and frequency between *Herschel* and *Planck* is not accidental: the two missions have been planned keeping in mind the added scientific value of a synergy between

⋆ *Herschel* is an ESA space observatory with science instruments provided by European-led Principal Investigator consortia and with important participation from NASA.
⋆⋆ Scottish Universities Physics Alliance.

them (Planck Collaboration 2006). In addition to providing a broader spectral coverage of common sources, the combination of *Planck* and *Herschel* data will be beneficial in other respects. In particular, the much higher resolution and sensitivity of *Herschel* makes it well-suited for follow-up studies of *Planck* sources[1], allowing us to assess the effects of source confusion in *Planck* channels. In some cases it will be possible to resolve individual detections by *Planck* into separated sources. More generally, *Herschel* will make it possible to quantify the boosting of *Planck* fluxes by the many faint sources within its beam. Moreover, *Herschel* data can be used to improve the foreground characterization, thus helping us to distinguish between genuine, possibly extragalactic, point sources and compact Galactic cirrus, and to provide more precise positions, essential for source identification at other wavelengths. This knowledge will be important for the interpretation of the all-sky *Planck* survey data. Note however that although *Herschel*'s resolution is much better than *Planck*'s, it is still highly likely that many of the *Herschel* 350 and 500 μm sources are also blends. H-ATLAS maps are in general not affected by source confusion, except in regions with considerable cirrus, but *Herschel* sources resolve to multiple MIPS (Multiband Imaging Photometer for *Spitzer*, Rieke et al. 2004) sources in many cases.

Also, a comparison between catalogues of galaxies observed with *Herschel* and *Planck* can be used as a check on the calibration of the two observatories, which is done in different ways. The absolute calibration of *Planck* fluxes should be better than 2% up to 353 GHz, where it is based on the CMB dipole, and $\simeq$7% in the two highest frequency channels (545 and 857 GHz), where it is based on a comparison with COBE/FIRAS (Planck HFI Core Team 2011; Zacchei et al. 2011)[2]. For comparison, the overall photometric accuracy of the *Herschel*/SPIRE instrument is conservatively estimated as $\simeq$7% (SPIRE Observers' Manual v2.2 2010)[3].

Owing to their different angular resolution and sensitivity, *Planck* and *Herschel* have almost complementary selection functions for extragalactic sources: *Planck* primarily detects nearby galaxies (although it might also detect extreme high-redshift objects), whereas most H-ATLAS galaxies lie around $z \sim 1$ (Eales et al. 2010). Moreover, *Planck* covers a broader spectral range (nine frequencies from 30 to 857 GHz), which is useful to improve the characterization and removal of foregrounds and to follow the spectral energy distributions (SEDs) of interesting objects, such as blazars, down to radio frequencies. With its all-sky coverage, *Planck* is ideal for detecting the rarest, most extreme (sub-)mm sources. In particular, it may detect the most luminous protoclusters of dusty galaxies, whose luminosities, integrated over the *Planck* beam, may be, at $z \gtrsim 1$, more than an order of magnitude higher than the mean luminosity of individual dusty galaxies at the same redshift (Negrello et al. 2005). The far superior *Herschel* resolution and point source detection capabilities will then allow us to establish the nature of candidate high-z protoclusters and to characterize the physical properties of those that are confirmed.

In this paper we present the results of a cross-correlation of the *Planck* ERCSC catalogue with the catalogue of H-ATLAS sources detected in the phase 1 fields (Dunne et al., in prep.). The common sources are described in Sect. 2. In Sect. 3 we compare the flux density estimates of both experiments. In Sect. 4 we study the contamination of the ERCSC subsample by looking for extended diffuse emission as a tracer of high-latitude cirrus. In Sect. 5 we discuss a very unusual source that may be a combination of a (maybe random) condensation of low redshift low-flux galaxies and a strongly lensed galaxy. Finally, in Sect. 6 we summarize our conclusions.

2. *Planck* sources in the H-ATLAS phase 1 fields

The *Planck* ERCSC (Planck Collaboration 2011b) provides an all-sky list of compact Galactic and extragalactic objects including stars with dust shells, prestellar cores, radio galaxies, blazars, infrared luminous galaxies, Galactic interstellar medium features, cold molecular cloud core candidates, and galaxy cluster candidates. The list contains more than 15 000 distinct objects, ~60% of which are visible in the *Planck* highest frequency (545 and 857 GHz) channels that virtually overlap with the *Herschel*/SPIRE bands. A sufficiently wide area survey made with *Herschel* is bound to contain at least some of these sources.

The H-ATLAS is the largest area survey carried out by the *Herschel* Space Observatory (Pilbratt et al. 2010). It will cover ~550 deg^2 with PACS (Poglitsch et al. 2010) and SPIRE (Griffin et al. 2010) in five bands, from 100 to 500 μm. The phase 1 observations have surveyed a sufficiently wide area (134.55 deg^2 at the moment of submitting this paper) to allow a preliminary, yet meaningful comparison with *Planck* ERCSC data.

The two highest frequency channels of the *Planck*/HFI practically overlap with the two lower frequency bands of *Herschel*/SPIRE. The 350 μm band almost coincides in central wavelength and bandwidth with the *Planck*/HFI 857 GHz channel. The 500 μm band and the *Planck*/HFI 545 GHz channel do not coincide exactly, but are close enough to consider a cross-check. The H-ATLAS phase 1 covers 134.55 deg^2 divided into three regions (GAMA-09, GAMA-12, and GAMA-15).

2.1. H-ATLAS 350 μm counterparts of ERCSC 857 GHz sources

Within the H-ATLAS phase 1 fields there are 28 ERCSC sources detected by *Planck* at 857 GHz. The positions of the 28 sources in the H-ATLAS GAMA-09, GAMA-12, and GAMA-15 fields are shown in Figs. 1–3 respectively. Among these, there are no clusters of galaxies (detected through the Sunyaev-Zel'dovich effect) or cold cores. Figures 5–7 show postage stamp images of these 28 sources as viewed by *Herschel* at 350 μm in the GAMA-09, GAMA-12, and GAMA-15 fields, respectively. By inspecting the SPIRE images around the positions of the sources we find several different situations.

As many as 16 out of the 28 ERCSC objects do not have a consistent H-ATLAS counterpart, because H-ATLAS sources within the *Planck* beam are too faint to explain the flux density measured by *Planck*. Almost all (15) of them are flagged as extended or have a relatively high ($\geq$0.125) cirrus flag in the ERCSC (11 have both properties). All but G266.26+58.99 (object #17 in Table 1 and (b) in Fig. 6 which, incidentally, is not flagged as extended and has a relatively low cirrus flag) are in

[1] For comparison, the resolution at the SPIRE 350 μm band is *FWHM* = 29.4 arcsec, whereas the ERCSC nominal beam at 857 GHz is 4.23 arcmin.

[2] This refers to the absolute calibration of the instrument. For individual sources, however, the uncertainty in the photometry is affected by other factors such as the uncertainty on the beam shape and the possibly extended nature of the source, leading to errors that can be as large as 30%, as cited by the Explanatory Supplement to the *Planck* ERCSC.

[3] The SPIRE Observers' Manual is available from the *Herschel* Science Centre:
herschel.esac.esa.int/Docs/SPIRE/pdf/spire_om.pdf

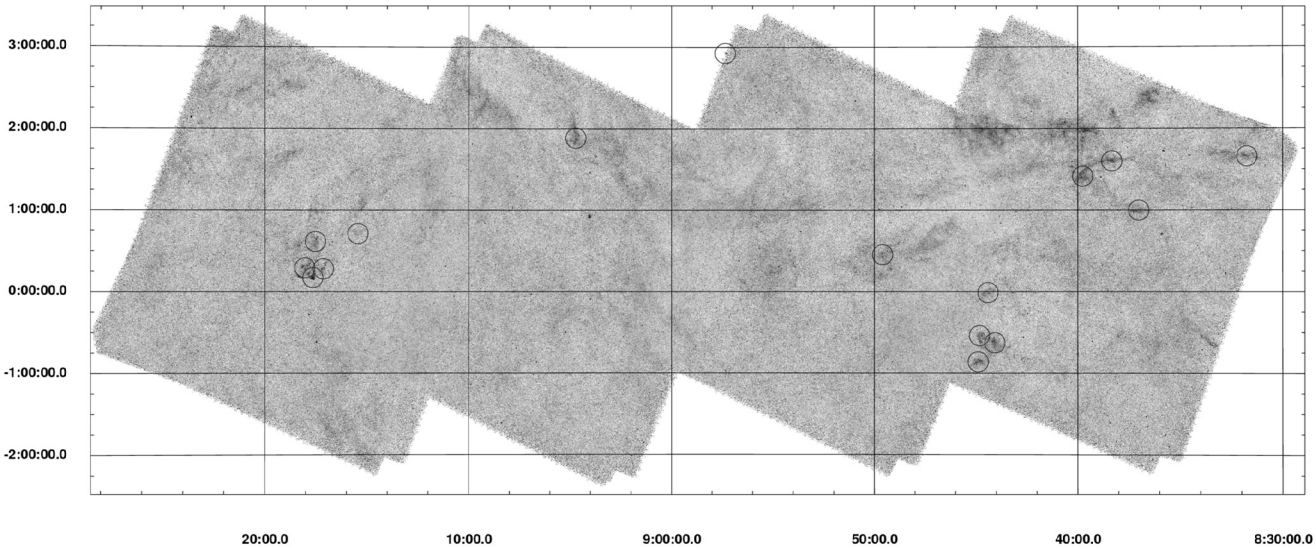

Fig. 1. Positions of the ERCSC 857 GHz sources in the 350 μm H-ATLAS GAMA-09 field. The source at coordinates 0857+3 has not been included in this analysis because it lies on the poorly sampled edge of the field.

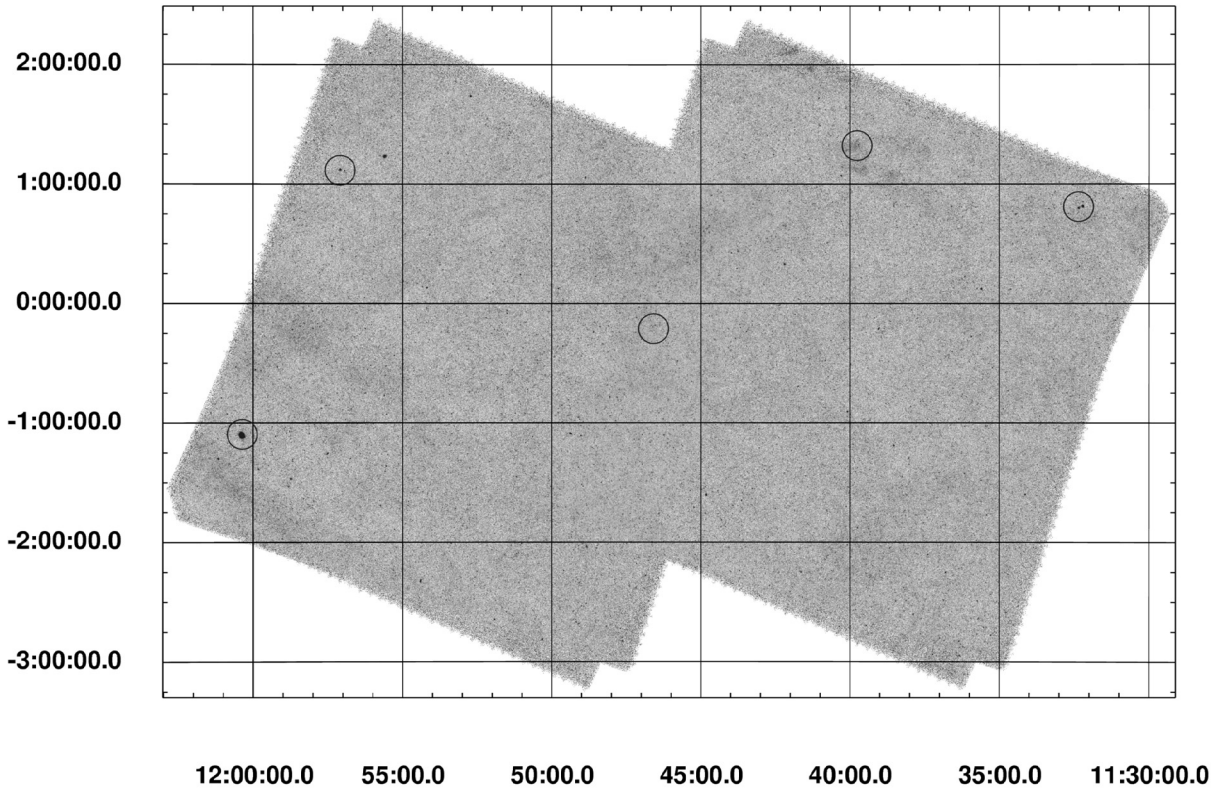

Fig. 2. Positions of the ERCSC 857 GHz sources in the 350 μm H-ATLAS GAMA-12 field.

the GAMA-09 field, which is more contaminated by Galactic emission than the other two GAMA fields. Figure 4 shows the positions of the ERCSC sources around the GAMA-09 field superimposed on the IRIS 100 micron map (Miville-Deschênes & Lagache 2005). The high correlation between ERCSC sources and the IRIS map reinforces the idea that the GAMA-09 ERCSC sources are likely to be mostly related to Galactic cirrus.

Of the other 12 sources, one (G263.84+57.55, #16 in Table 1 and object (a) in Fig. 6) is clearly resolved by *Herschel* into two relatively bright sources, the galaxy pair KPG289 (Karachentsev et al. 1976) formed by the galaxies NGC 3719 and NGC 3720, each with flux density >250 mJy at 350 μm, while another object (G270.59+58.52, object #18 in Table 1, which is shown in panel (c) of Fig. 6) is resolved into an unusual condensation of low flux, probably high-redshift point sources. We will discuss this source in more detail in Sect. 5. Finally, 10 ERCSC sources can be clearly identified with single bright H-ATLAS sources at low redshift, including the edge-on spiral NGC 5746 (object (h) in Fig. 7) the spirals NGC 5690, NGC 5705 and NGC 4030, the peculiar asymmetric galaxy NGC 5713 (Dale et al. 2012), in addition to the above mentioned pair NGC 3719 and NGC 3720.

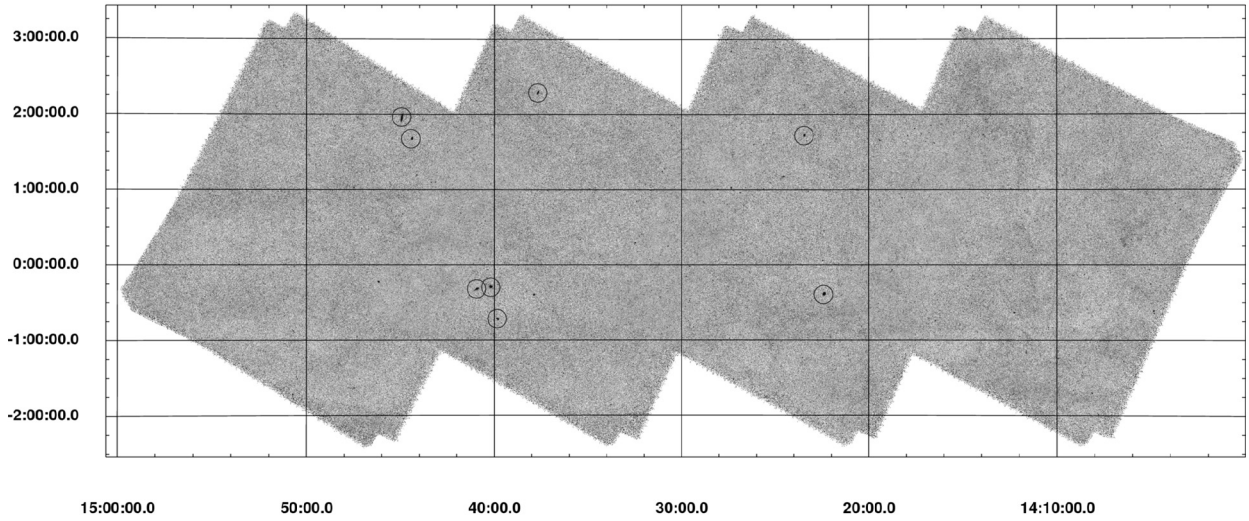

Fig. 3. Positions of the ERCSC 857 GHz sources in the 350 μm H-ATLAS GAMA-15 field.

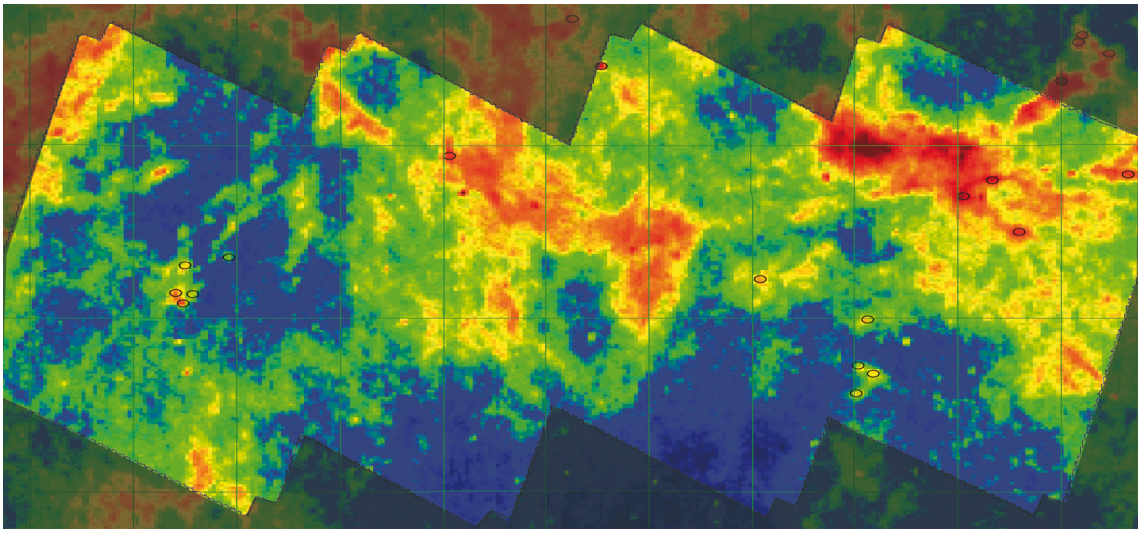

Fig. 4. Position of the ERCSC sources (black ovals) superimposed on the IRIS 100 micron map around the GAMA-09 H-ATLAS field.

Table 1 lists the 28 sources with their 857 GHz flux densities taken from the ERCSC (Planck Collaboration 2011). The table gives the ERCSC source name, the RA and Dec coordinates, the flux densities and associated errors, and the EXTENDED and CIRRUS flags. Column 9 gives the 350 μm flux densities of the brightest H-ATLAS sources found inside the *Planck* beam[4], provided that they have $S_{350} \geq 250$ mJy. For these sources we give, in Col. 11, the spectroscopic or photometric redshifts taken from the H-ATLAS catalogue (Dunne et al., in prep.).

2.2. H-ATLAS 500 μm counterparts of ERCSC 545 GHz sources

There are 14 ERCSC sources detected at 545 GHz that lie in the H-ATLAS phase 1 fields. Among them, 13 are also in the sample of 28 sources detected by the ERCSC at 857 GHz that we described in Sect. 2.1. The remaining object (PLCKERC545 G230.17+32.05, with ID #29 in Table 2) is in the GAMA-09 region and has a high CIRRUS flag. Like at 857 GHz, more than half of the sources (8 out of 14, 7 of them being in the GAMA-09 field) do not have a plausible H-ATLAS counterpart. Table 2 lists the 14 sources, giving the H-ATLAS ID and redshifts for the six sources that have a 500 μm counterpart with $S_{500} \gtrsim 250$ mJy.

3. Photometry

Comparing the flux density estimations of the ERCSC and the SPIRE phase 1 catalogues is not straightforward. To correctly compare ERCSC and SPIRE photometric estimations it is necessary to take into account that

- *Herschel* has better angular resolution than *Planck*. It is possible that an ERCSC source can be resolved into several sources by *Herschel*.
- The wavelengths of the *Planck* bands do not correspond exactly to the wavelenghts of their *Herschel* counterparts.
- Both catalogues have been obtained by using different detection and photometry extraction algorithms.

The effect of the different angular resolutions can be corrected, at least to first order, by integrating the SPIRE flux densities over

[4] Unless otherwise stated, the beam is a circle with radius $r = FWHM/2\sqrt{2\log 2}$.

Table 1. ERCSC sources at 857 GHz and their H-ATLAS counterparts (inside a 4.23 arcmin radius circle around the ERCSC position) at 350 μm.

ID	ERCSC name	RA (deg)	Dec (deg)	$S_{857\ \mathrm{GHz}}$ (Jy)	$\Delta S_{857\ \mathrm{GHz}}$ (Jy)	EXT	Cirrus	H-ATLAS ID	Other ID	$S_{350\ \mu\mathrm{m}}$ (Jy)	$\Delta S_{350\ \mu\mathrm{m}}$ (Jy)	z_{spec}	D (arcmin)
1	G223.40+22.96	127.935	1.659	10.751	1.940	1	0.219						
2	G224.33+24.38	129.583	1.602	9.924	1.209	1	0.188						
3	G224.70+24.60	129.940	1.415	6.077	0.894	1	0.156						
4	G224.73+23.79	129.253	0.998	8.440	1.650	1	0.156						
5	G226.70+24.89	131.101	–0.013	6.987	1.392	1	0.125						
6	G226.98+26.25	132.398	0.454	6.256	1.261	1	0.109						
7	G227.24+24.51	131.018	–0.629	7.291	0.895	1	0.125						
8	G227.26+24.72	131.206	–0.540	3.234	0.917	1	0.125						
9	G227.58+24.57	131.222	–0.863	8.093	1.194	1	0.125						
10	G227.75+30.24	136.180	1.886	13.259	2.118	1	0.078						
11	G230.55+31.91	138.859	0.711	1.535	0.406	0	0.125						
12	G230.97+32.31	139.381	0.614	0.872	1.232	1	0.125						
13	G231.25+32.05	139.284	0.279	3.429	0.769	1	0.125						
14	G231.38+32.24	139.511	0.291	2.863	2.249	1	0.125						
15	G231.43+32.10	139.413	0.173	4.038	0.539	0	0.125						
16	G263.84+57.55	173.088	0.810	1.990	0.434	0	0.047	J113221.5+004814	NGC 3720	1.2149	0.0364	0.0198	0.405
								J113213.3+004907	NGC 3719	1.0098	0.0345	0.0195	1.998
17	G266.26+58.99	174.940	1.323	2.056	0.667	0	0.062						
18	G270.59+58.52	176.646	–0.211	2.145	0.824	1	0.031	J114637.9-001132	G12H29	0.3783	0.0074	3.259	1.359
19	G274.04+60.90	179.271	1.115	1.511	0.380	0	0.109	J115705.9+010730	CGCG 013-010	1.2073	0.0304	0.0395	0.628
20	G277.37+59.21	180.100	–1.104	17.578	0.441	0	0.047	J120023.2-010600	NGC 4030	18.3014	0.1060	0.0048	0.303
21	G345.11+54.84	215.605	–0.395	3.361	0.466	0	0.016	J142223.4-002313	NGC 5584	3.9080	0.0565	0.0055	0.645
22	G347.77+56.35	215.865	1.720	1.329	0.447	0	0.031	J142327.2+014335	UGC9215	1.6225	0.0584	0.0046	0.412
23	G350.46+51.85	219.962	–0.716	2.235	0.596	0	0.078	J143949.5-004305	NGC 5705	1.4737	0.0565	0.0059	0.381
24	G351.01+52.11	220.048	–0.298	7.824	0.635	0	0.078	J144011.1-001725	NGC 5713	7.7971	0.0739	0.0063	0.474
25	G351.22+51.97	220.238	–0.320	4.881	0.476	0	0.078	J144056.2-001906	NGC 5719	5.6896	0.1303	0.0057	0.231
26	G353.15+54.45	219.422	2.288	6.179	0.506	0	0.062	J143740.9+021729	NGC 5690	6.4066	0.0855	0.005847	0.239
27	G354.50+52.84	221.113	1.676	2.942	0.511	0	0.078	J144424.3+014046	NGC 5740	2.8600	0.0474	0.0052	0.722
28	G354.96+52.95	221.237	1.951	11.238	0.560	0	0.062	J144455.9+015719	NGC 5746	7.9449	0.1451	0.0057	0.359

Notes. *Planck* flux densities and their associated errors are taken from the ERCSC GAUFLUX column.
Only the H-ATLAS sources with flux density $S_{350\ \mu\mathrm{m}} > 0.3$ Jy have been included in the table (blank spaces mean that no H-ATLAS source brighter than 0.3 Jy at 350 μm are associated to the ERCSC detection). Object PLCKERC G263.84+57.55 is a blend of 2 H-ATLAS sources, each with $S_{350\ \mu\mathrm{m}} > 0.3$ Jy. All redshifts are spectroscopic. In the case of G270.59+58.52 the redshift refers to the strongly lensed galaxy G12H29.

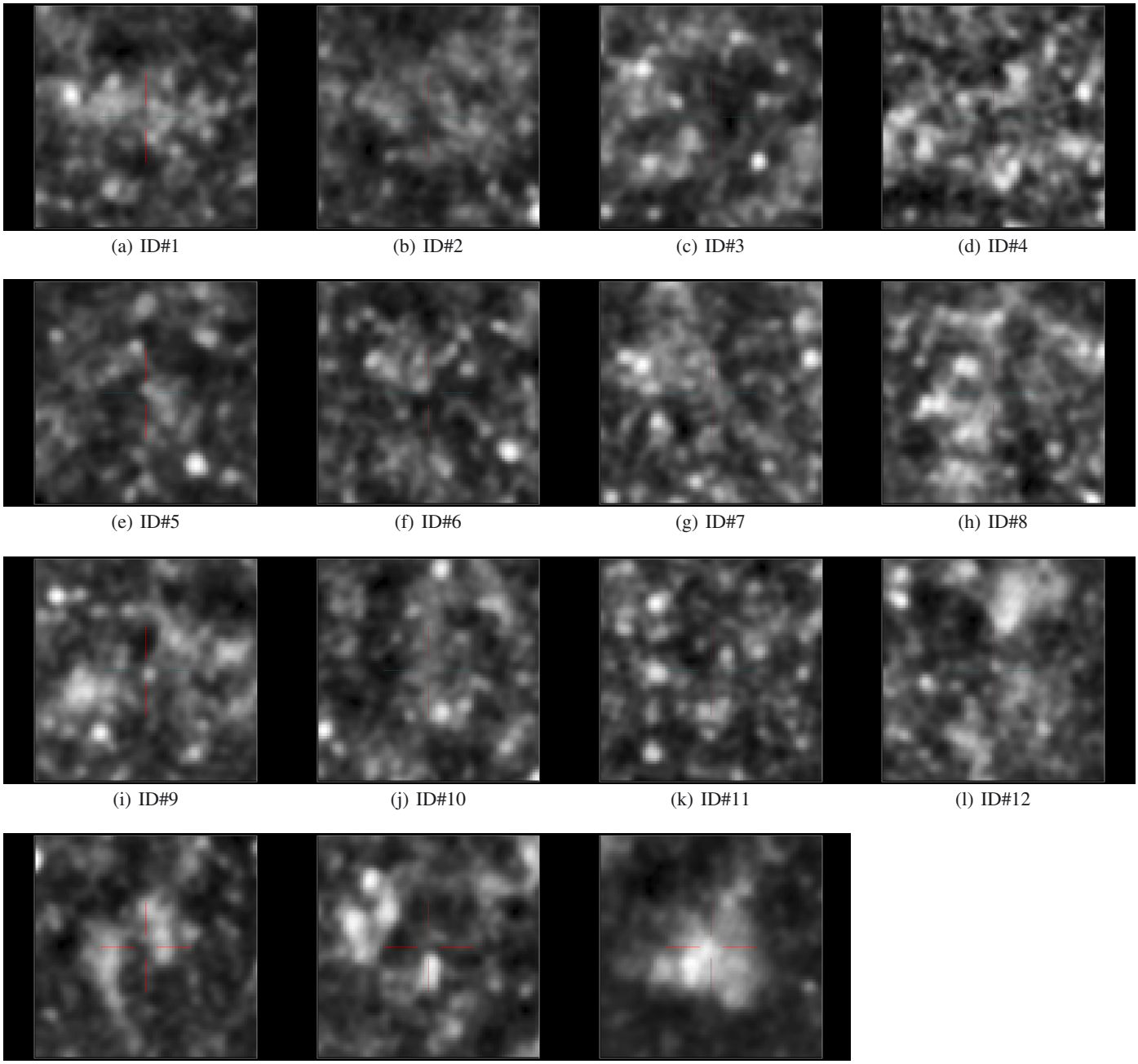

(a) ID#1 (b) ID#2 (c) ID#3 (d) ID#4

(e) ID#5 (f) ID#6 (g) ID#7 (h) ID#8

(i) ID#9 (j) ID#10 (k) ID#11 (l) ID#12

(m) ID#13 (n) ID#14 (o) ID#15

Fig. 5. SPIRE images at 350 μm showing postage stamps of the *Planck* ERCSC sources at 857 GHz in the H-ATLAS GAMA-09 field. The images are 400 arcsec wide and the red crosses indicate the ERCSC position for each source. The full ERCSC name of the objects has been abbreviated in the captions for conciseness.

the larger *Planck* beam area and weighting by the *Planck* beam response. The effect of the different central wavelenghts can be taken into account by means of SED colour correction, as will be described in Sect. 3.2. A review of the technical details of the ERCSC and SPIRE flux density estimates used in the catalogues is beyond the scope of this work. ERCSC photometry is described in Planck Collaboration (2011b) and Aatrokoski et al. (2011); SPIRE photometry is described in Rigby et al. (2011); both catalogues have passed strict internal and external validation. For pointlike sources, we assume that the flux density estimates that are given in both catalogues are accurate, within the calibration uncertainties of their experiments. However, it must be noted that the different ways in which the photometry of extended sources is obtained in the ERCSC and in the H-ATLAS phase 1 catalogues can affect the comparison. The H-ATLAS catalogues use aperture photometry scaled to the optical size of the sources (Rigby et al. 2011). The *Planck* ERCSC contains several types of photometric measurements for each source; the default aperture photometry information is listed in the ERCSC "FLUX" column, but other photometric measurements may be more appropriate in certain circumstances. As described in the *Planck* Explanatory Supplement to the ERCSC (Aatrokoski et al. 2011), for extended sources it may be better to use the Gaussian-fit photometry

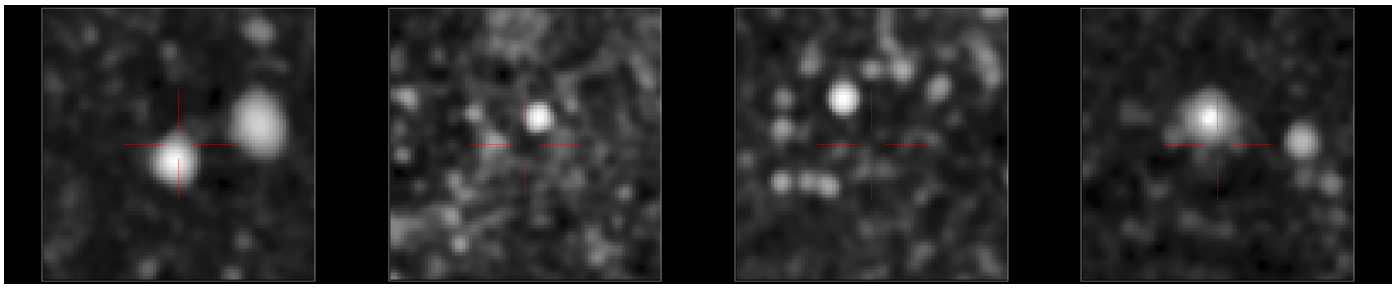

(a) ID#16 (b) ID#17 (c) ID#18 (G270.59+58.52) (d) ID#19

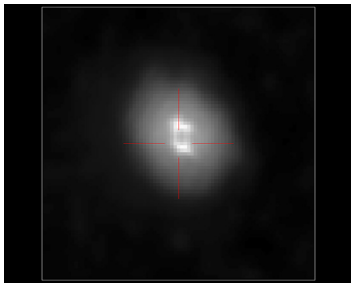

(e) ID#20

Fig. 6. SPIRE images at 350 μm showing postage stamps of the *Planck* ERCSC sources at 857 GHz in the H-ATLAS GAMA-12 field. The images are 400 arcsec wide and the red crosses indicate the ERCSC position for each source.

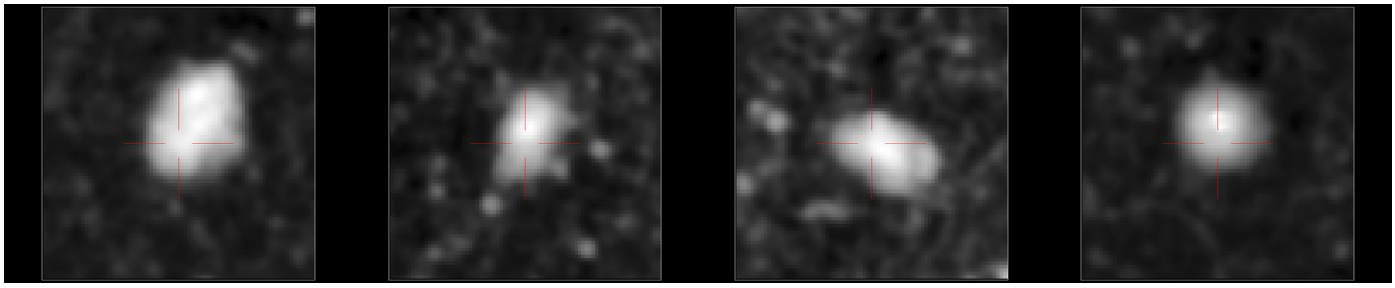

(a) ID#21 (b) ID#22 (c) ID#23 (d) ID#24

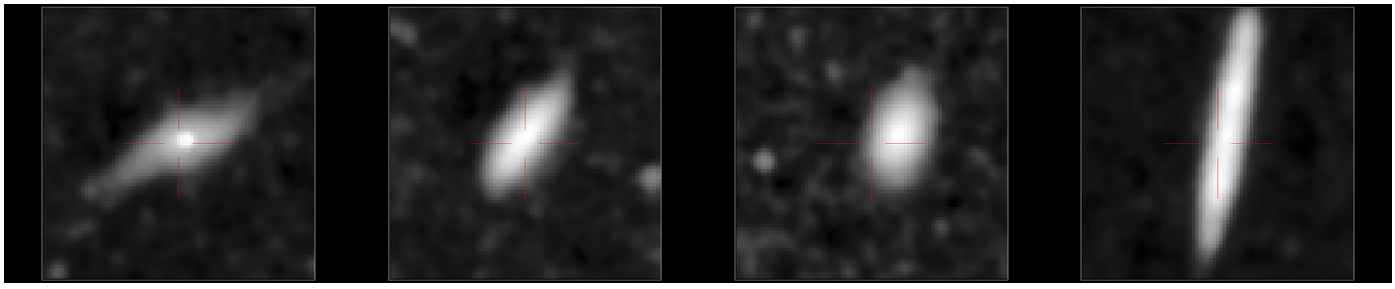

(e) ID#25 (f) ID#26 (g) ID#27 (h) ID#28

Fig. 7. SPIRE images at 350 μm showing postage stamps of the *Planck* ERCSC sources at 857 GHz in the H-ATLAS GAMA-15 field. The images are 400 arcsec wide and the red crosses indicate the ERCSC position for each source.

listed in the ERCSC "GAUFLUX" column instead of a fixed aperture photometry. Since a significant fraction of the sources in our sample at 857 GHz are flagged as extended in the ERCSC, we have compared the H-ATLAS flux densities to both the fixed aperture photometry ("FLUX") and the Gaussian-fit ("GAUFLUX") ERCSC flux densities. We find that at the lowest fluxes FLUX and GAUFLUX work similarly well, while at bright fluxes GAUFLUX is more consistent with *Herschel* photometry (maybe because many bright ERCSC sources are extended). Therefore, for the remainder of this paper, we will use GAUFLUX when referring to *Planck* photometry.

3.1. ERCSC-857 GHz and H-ATLAS 350 μm flux densities

According to the technical specifications of their respective instruments, the *Planck*/HFI 857 GHz and the *Herschel*/SPIRE 350 μm channels have almost exactly the same central

Table 2. ERCSC sources at 545 GHz and their H-ATLAS 500 μm counterparts inside a 4.47 arcmin radius circle around the ERCSC position.

ID	Name	RA (deg)	Dec (deg)	$S_{545\,\mathrm{GHz}}$ (Jy)	$\Delta S_{545\,\mathrm{GHz}}$	EXT	CIRRUS	H-ATLAS ID	Other ID	$S_{500\,\mu\mathrm{m}}$ (Jy)	$\Delta S_{500\,\mu\mathrm{m}}$ (Jy)	z_{spec}	D (arcmin)
3	G224.70+24.61	129.951	1.422	1.543	0.517	0	0.156						
6	G226.97+26.25	132.394	0.458	2.185	0.647	1	0.109						
8	G227.27+24.71	131.198	–0.550	3.718	1.536	1	0.125						
9	G227.57+24.56	131.215	–0.863	4.234	1.194	1	0.125						
10	G227.77+30.23	136.181	1.869	4.554	1.168	1	0.078						
29	G230.17+32.05	138.809	1.055	1.191	0.463	0	0.141						
13	G231.44+32.10	139.420	0.174	1.410	0.389	0	0.125						
18	G270.59+58.54	176.648	–0.199	1.358	0.610	0	0.031	J114637.9-001132	G12H29	0.298	0.008	3.259	0.746
20	G277.36+59.21	180.094	–1.097	4.546	0.419	0	0.047	J120023.2-010600	NGC 4030	5.661	0.052	0.0048	0.229
21	G345.12+54.85	215.603	–0.381	1.151	0.415	0	0.016	J142223.4-002313	NGC 5584	1.441	0.033	0.0055	0.460
24	G351.01+52.12	220.047	–0.292	2.213	0.524	0	0.078	J144011.1-001725	NGC 5713	2.278	0.035	0.0063	0.141
25	G351.21+51.96	220.242	–0.327	1.275	0.439	0	0.078	J144056.2-001906	NGC 5719	1.817	0.073	0.0057	0.729
26	G353.14+54.45	219.414	2.290	1.551	0.433	0	0.062	J143740.9+021729	NGC 5690	2.210	0.046	0.0855	0.409
28	G354.97+52.95	221.236	1.956	3.456	0.534	0	0.062	J144455.9+015719	NGC 5746	2.686	0.081	0.0058	0.204

Notes. *Planck* flux densities and their associated errors are taken from the ERCSC GAUFLUX column.
Only the H-ATLAS sources with flux density $S_{500\,\mu\mathrm{m}} \gtrsim 0.3$ Jy have been included in the table (blank spaces mean that no H-ATLAS source brighter than 0.3 Jy at 500 μm are associated to the ERCSC detection). In the case of G270.59+58.54 the redshift refers to the strongly lensed galaxy G12H29. The ID numbers correspond to the counterparts of these objects in Table 1, except for the case of G230.17+32.05 which has no clear counterpart in that table.

wavelength and roughly the same bandwidth. This makes it easy to directly compare the flux density estimations of the ERCSC sources present in the H-ATLAS fields. To take into account the different angular resolutions of *Herschel* and *Planck*, we calculated an effective *Herschel* 350 μm flux density by summing the flux densities, corrected for the effect of the *Planck* beam, of the sources listed in the H-ATLAS phase 1 catalogue around the ERCSC positions. We assumed a circular, Gaussian beam of $FWHM = 4.23$ arcmin (Planck Collaboration 2011b).

Figure 8 shows the *Planck* 857 GHz flux densities compared to *Herschel* 350 μm flux densities for those ERCSC sources that have at least one $S_{\mathrm{H-ATLAS}} \geq 250$ mJy. All these sources lie in the GAMA-12 or GAMA-15 fields. According to Aatrokoski et al. (2011), the ERCSC flux densities below $\simeq$1.3 Jy are boosted by the well-known selection bias (sources sitting on top of positive noise plus confusion plus Galactic emission fluctuations that dominate the contribution to the measured flux densities are more likely to be detected). Excluding the large edge-on spiral NGC 5746, which will be discussed below, for sources with H-ATLAS 350 μm flux densities $\geq$1.5 Jy we see a good agreement between *Herschel* and *Planck* flux densities. We find $\langle S_{\mathrm{H-ATLAS}} - S_{\mathrm{ERCSC}} \rangle \simeq 0.1$ Jy. The relative flux density difference for the same sources, defined as

$$\epsilon = 100 \times \left\langle \frac{S_{\mathrm{H-ATLAS}} - S_{\mathrm{ERCSC}}}{S_{\mathrm{H-ATLAS}}} \right\rangle, \quad (1)$$

is $|\epsilon| = 3\%$, smaller than the calibration uncertainty of both *Herschel* and *Planck*. However, the relative difference of the individual sources shows a large ($\sim$20%) scatter, probably due to the small size of the sample. The mean difference between the ERCSC and H-ATLAS positions for sources brighter than 1.5 Jy is 0.42 arcmin, with a dispersion of 0.17 arcmin. For the assumed beam shape, this may account for a $\simeq$5% underestimate of ERCSC flux densities.

The two remarkable outliers in Fig. 8 are sources #18 and #28 in Table 1. Source #18, G270.59+58.52 (object (c) in Fig. 6), flagged as extended in the ERCSC and with $S_{\mathrm{H-ATLAS}} = 352$ mJy, will be discussed in Sect. 5. Source #28 (object (h) in Fig. 7) is identified as NGC 5746, a large edge-on spiral that is clearly resolved as a very extended source by SPIRE but is not flagged as extended by the ERCSC. We believe that the discrepancy between the flux densities for this object reported by H-ATLAS and the ERCSC is due to the very different angular resolution of *Herschel* and *Planck* and to the different way in which background subtraction has been performed by the catalogue-making pipelines of the two experiments. In particular, if aperture photometry is applied to the raw (not background-subtracted) SPIRE 350 micron map, a flux density of $\sim$10 Jy

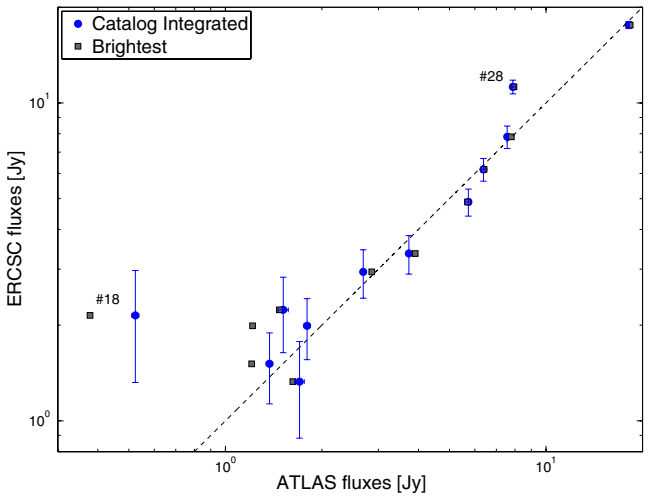

Fig. 8. ERCSC 857 GHz flux densities compared with the 350 μm flux densities of the brightest H-ATLAS sources inside the *Planck* beam (squares). The dashed line indicates the $S_{\mathrm{ATLAS}} = S_{\mathrm{ERCSC}}$ identity. The filled circles show the summed flux densities, weighted with a Gaussian beam centred on the ERCSC position and with $FWHM = 4.23$ arcmin (Planck Collaboration 2011b). Only the ERCSC sources with at least one *Herschel* counterpart with flux density $S_{\mathrm{H-ATLAS}} > 0.25$ Jy are shown in this plot (see text for further details). The outlier with ERCSC flux density $\sim$10 Jy is the edge-on spiral galaxy NGC 5746 (object #28 in Table 1, see discussion in the main text). The outlier with ERCSC flux density $\sim$2 Jy is the G12H29 (source #18 in Table 1), to be discussed in Sect. 5.

is obtained for this object, which is more consistent with the 857 GHz value. A revised version of the phase I H-ATLAS catalogue, which deals more carefully with very extended sources, solves this discrepancy (L. Dunne, priv. comm.).

3.2. ERCSC-545 GHz and H-ATLAS 500 μm flux densities

The comparison between the *Planck* 545 GHz and the SPIRE 500 μm flux densities is less straightforward. The central frequency of the 500 μm channel is ~600 GHz, significantly higher than that of the nearest *Planck* channel (545 GHz). A colour correction is thus necessary. From the mean SED of IRAS PSCz galaxies determined by Serjeant & Harrison (2005), we find $\langle S_{600}/S_{545}\rangle \simeq 1.35$. For the comparison with *Planck* we scaled down the H-ATLAS flux densities by this factor, except for the rich clump of low-flux galaxies, for which we adopted a correction factor of 1.1 for the strongly lensed galaxy at $z = 3.259$ and of 1.3 for the surrounding H-ATLAS sources, assumed to be at $z \leq 1$. These factors were calculated using the SED of H-ATLAS J142413.9+022304, a strongly lensed sub-mm galaxy at $z \approx 4.24$ (Cox et al. 2011), for the strongly lensed galaxy and the SED of SMM J2135-0102 ("The Cosmic Eyelash"; Ivison et al. 2010; Swinbank et al. 2010), that Lapi et al. (2011) found to work well for many high-z H-ATLAS galaxies. We denote the colour-corrected flux by the symbol S^*.

Figure 9 compares the *Planck* 545 GHz flux density with that of the brightest source inside the *Planck* beam (filled squares) and with that obtained summing the flux densities of H-ATLAS sources within the *Planck* beam, corrected for the effect of the beam response (*FWHM* = 4.47 arcmin) function and the colour correction (filled circles). Only the *Planck* ERCSC 545 GHz sources that have at least one H-ATLAS counterpart with (not colour-corrected) $S_{\rm H-ATLAS} \gtrsim 250$ mJy are shown in the plot. Again NGC 5746 and the clump around G270.59+58.52 stand out for their high ERCSC-to-H-ATLAS flux density ratios. Excluding these, we find, after the colour correction, $\langle S^*_{\rm H-ATLAS} - S_{\rm ERCSC}\rangle = -0.16$ Jy, with a dispersion of ≃0.25 Jy for sources with $S^*_{\rm H-ATLAS} > 1$ Jy. The corresponding relative difference is $\langle\epsilon\rangle = -7.5\%$ with dispersion $\sigma_\epsilon = 13.5\%$. This result, however, was obtained from a very small sample of five sources and cannot be considered to be statistically meaningful.

4. Contamination by Galactic cirrus

The GAMA-09 field is more contaminated by Galactic emission than the other two GAMA fields (Bracco et al. 2011). None of the 15 ERCSC 857 GHz sources, in this field with $S_{\rm ERCSC}$ in the range 1.2−3.5 Jy, have a plausible *Herschel* counterpart. The summed flux densities of the faint *Herschel* sources within the *Planck* beam fall well short of accounting for the ERCSC flux densities. A visual inspection of Fig. 5 clearly reinforces the idea that the ERCSC sources in this region of the sky are not associated with bright *Herschel* galaxies. All but two of the ERCSC sources in the GAMA-09 have a cirrus flag ≥0.125 and all but two (different from the previous two objects) are labelled as extended in the ERCSC. It is thus likely that most of the flux density within the *Planck* beam comes from Galactic cirrus. The situation is much better in the GAMA-12 and GAMA-15 fields. In the former, only one (out of five) 857 GHz ERCSC source does not have an H-ATLAS counterpart with $S_{\rm H-ATLAS} > 250$ mJy. Somewhat surprisingly, this source is not labelled as extended in the ERCSC and has a relatively low cirrus flag (0.0625). One of the two ERCSC 545 GHz sources in the same field behaves in a similar way: no H-ATLAS counterpart with $S_{\rm H-ATLAS} > 250$ mJy, not labelled as extended, low cirrus flag (0.03125). Fortunately, all the eight 857 GHz and the five 545 GHz ERCSC sources in the GAMA-15 field do have a consistent H-ATLAS counterpart.

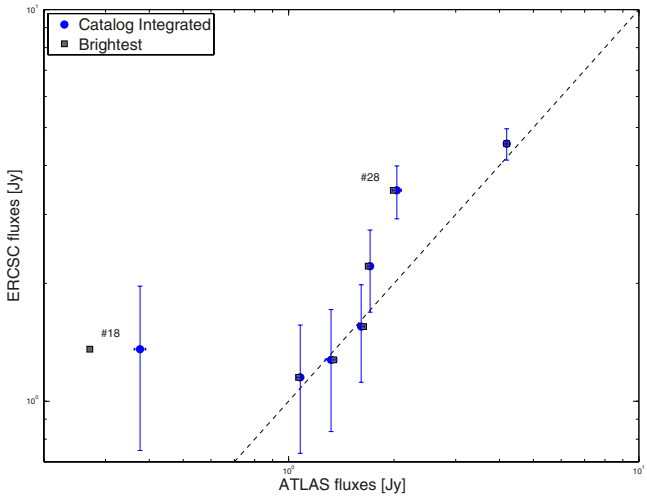

Fig. 9. ERCSC flux densities at 545 GHz compared with the colour-corrected 500 μm flux densities of the brightest H-ATLAS sources inside the *Planck* beam (squares). The dashed line indicates the $S_{\rm ATLAS} = S_{\rm ERCSC}$ identity. The filled circles show the colour-corrected summed flux densities, weighted with a Gaussian beam centred on the ERCSC position and with *FWHM* = 4.47 arcmin (Planck Collaboration 2011b). Only the ERCSC sources with at least one *Herschel* counterpart with (not colour-corrected) flux density $S_{\rm H-ATLAS} > 0.25$ Jy are shown in this plot. The outlier with ERCSC flux density ~3.5 Jy is the edge-on spiral galaxy NGC 5746. The outlier with ERCSC flux density ~1.5 Jy is the G12H29 source to be discussed in Sect. 5.

Although the statistics are poor, these findings may indicate that all ERCSC sources with a cirrus flag ≥0.125 are cirrus dominated, even if they are not labelled as extended, as is the case for two 857 GHz and three 545 GHz GAMA-09 sources. Of the three 857 GHz sources labelled as extended but with a cirrus flag <0.125, two are probably cirrus dominated, while the third is the composite high-z lensed galaxy plus low-z clump (see Sect. 5). All 545 GHz sources labelled as extended are probably cirrus dominated, even if the cirrus flag is <0.125.

We can then tentatively conclude that a cirrus flag ≥0.125 *or* the "extended" label are good indicators of cirrus dominance, although their presence (or absence) does not always guarantee that a source is (or is not) dominated by cirrus.

5. The strongly lensed *Herschel*/*Planck* source H-ATLAS J114637.9-001132 at $z = 3.26$

The ERCSC object # 18, PLCKERC857 G270.59+58.52, shown as observed by *Herschel* in panel (c) of Fig. 6 and in Fig. 10, has some unusual characteristics that make it interesting and worthy of further study. Eleven out of the 12 matches between ERCSC sources found at 857 GHz and H-ATLAS sources with $S_{\rm H-ATLAS} > 250$ mJy are associated with nearby quiescent galaxies detected in the optical. One source, however, has no bright optical counterpart. Instead, it is associated with a clump of sources with low *Herschel* flux densities (as can be better appreciated in Fig. 11) grouped around a bright *Herschel* source, HATLAS J114637.9-001132, alias G12H29, whose flux peaks at 350 μm. Its *Planck* colour is also unusual, as can be

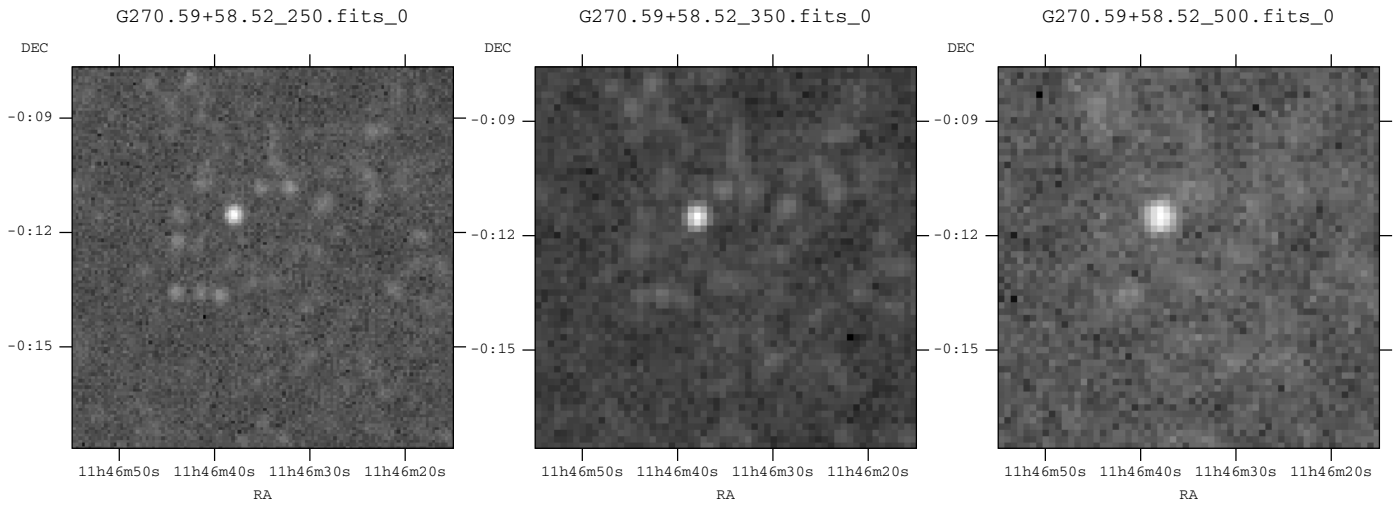

Fig. 10. Clump around G12H29 as seen by *Herschel* at 250 (*left*), 350 (*centre*) and 500 μm (*right*). The field of view is 600 arcsec wide and is centred at the position of the 857 GHz ERCSC source PLCKERC857 G270.59+58.52.

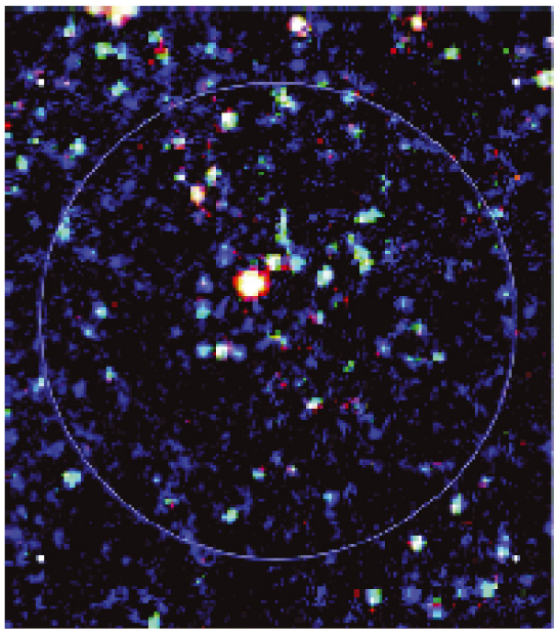

Fig. 11. *Herschel* three-colour image of the region around HATLAS J114637.9-001132 (alias G12H29). Colours are: blue – 250 μm; green – 350 μm; red – 500 μm. The colour scale was chosen so that objects that are red/white are likely to lie at $z \sim 3$. The brightest such object in this image is the $z = 3.259$ likely lensed galaxy HATLAS J114637.9-001132. The circle is centred on the *Planck* source and is the size of the *Planck* 857 GHz beam. (This figure is available in color in the electronic form.)

seen in Fig. 12 where G12H29 is indicated by a red dot. This source was already a target for spectroscopic sub-mm follow-up of candidate lensed galaxies (see e.g. Negrello et al. 2010). A CO spectroscopic redshift of $z = 3.259$ has been obtained for this source (Harris et al. 2012; Van der Werf et al., in prep.). Recent LABOCA data do suggest the presence of other sources in the same clump with SPIRE-to-870 flux ratios that match those of the $z = 3.26$ source, providing indirect evidence for other sources associated with it at the same redshift (Clements et al., in prep.).

The SDSS DR7 (Abazajian et al. 2009) shows a dense clump just on top of G12H29. Fu et al. (2012) have studied G12H29 and the SDSS clump in detail and determined the lensing nature of HATLAS J114637.9-001132 during a Keck laser guide star adaptive optics imaging (J and K_s-band) programme of bright *Herschel* 500 μm sources from H-ATLAS. The K_s-band image shows complex filamentary structures that do not appear at J-band. Observations with the SubMillimeter Array (SMA) reveal two 880 μm sources with flux densities of 31 mJy and 27 mJy, separated by 3″. In their work, Fu et al. (2012) show that the observations can be nicely explained by a lens model in which the lens is a rather complex system located at $z \sim 1$. The photometric redshifts of the optical sources around the lensed object have been determined using SDSS *ugriz* + UKIDSS *YJHK* photometry using the publicly available photo-z code EAZY (Brammer et al. 2008). The Keck K-band data were not used for the photo-z calculation. For the two central lensing galaxies, their blended photometry indicates a photo-z of 1.076 (the 68% confidence interval is 0.982 to 1.305), which is substantially higher than the SDSS DR8 photo-z (0.71). For a more detailed discussion on the lens, the reader is referred to Fu et al. (2012).

Apart from the SDSS clump already described, there is an unusually rich condensation of other low-flux H-ATLAS objects within the *Planck* beam centred on G12H29. Several of these sources have red *Herschel* colours. We have determined photometric redshifts for these objects using the SMM J2135-0102 SED, that was shown to work quite well for $z \geq 1$ (González-Nuevo et al. 2012; Lapi et al. 2011). We find that four out of the six H-ATLAS sources that are located inside a circle of radius $\sigma_{857} = 4.23/2\sqrt{2\log 2}$ arcmin (Planck Collaboration 2011b) centred on G12H29 have $0.75 < z_{\rm phot} < 1.25$. We checked that other photo-z methods (e.g. Clements et al., in prep.) produce answers that are broadly consistent with those from the Lapi et al. (2011) method. However, these photo-z are calculated using only the three SPIRE bands and are therefore uncertain. For those H-ATLAS objects that can be matched to SDSS galaxies, we recalculated the photo-z using the optical data. Our results seem to indicate that most of these clump sources have lower redshifts $\langle z \rangle < 0.3$ than estimated using SPIRE data alone.

To test if the overdensity we observe around HATLAS J114637.9-001132 is statistically significant, we randomly selected 1000 *Herschel* sources and counted the number of galaxies in circles with the same radius σ_{857}. The median

number of neighbours is 1, with a standard deviation of 1.2. None of the sources in the control sample has a number of neighbours equal to or larger than H-ATLAS J114637.9-001132.

Following a bootstrap-type argument and realizing that we can divide the survey area into 30 257 independent cells of size σ_{857} around H-ATLAS sources (ordered downwards in flux density at 350 microns), we counted the number of H-ATLAS sources inside each one of these cells. We find that the fraction of cells as populated as the G12H29 clump, or more, is 9.915×10^{-4} (30 cells). Using a Bayesian approach and the binomial distribution (Wall & Jenkins 2003), we find that the 99.99% confidence interval for that fraction is $[0.4422 \times 10^{-4}, 1.8736 \times 10^{-3}]$ (narrowest interval that includes the mode and encompasses 99.99% cases, S. Andreon, priv. comm.). We conclude that the overdensity observed around G12H29 is statistically significant, but given our limited knowledge about the redshift distribution of the clump objects it is unclear whether the clump is a real association of objects at the same redshift or a random alignment of galaxies at very different distances. Our current data seem to favour this last interpretation (a low-redshift clump at $z < 0.3$ plus the lens SDSS clump at $z \sim 1$ plus the lensed galaxy at $z = 3.259$), but the large uncertainties of photo-z estimates make it impossible to rule out other possibilities at this point.

The large *Planck* beam means that there is considerable potential for source confusion to affect the colours. The H-ATLAS survey has detected at $\geq 5\sigma$ in the *Herschel* 350 μm band (equivalent to the *Planck* 857 GHz channel), sources with a total flux density of $S_{\rm H-ATLAS} = (0.52 \pm 0.01)$ Jy (taking into account the effect of a Gaussian beam with $FWHM = 4.23$ arcmin centred on the *Planck* position) to be compared with the ERCSC flux density $S_{\rm ERCSC} = 2.15 \pm 0.83$ Jy. Again allowing for the effect of the *Planck* beam (with $FWHM = 4.47$ arcmin in this case), the summed contributions of $\geq 5\sigma$ H-ATLAS sources at 500 μm is $S_{\rm H-ATLAS} = (0.44 \pm 0.02)$ Jy. Applying a colour correction of a factor of 1.1 for G12H29 and 1.3 for the other sources (assumed to be at redshift ≤ 1), we obtain $S^*_{\rm H-ATLAS} = (0.38 \pm 0.01)$ Jy, compared with $S_{\rm ERCSC} = (1.36 \pm 0.61)$ Jy. This suggests that *Planck* measurements are boosted by a positive background fluctuation, which may also account for the fact that only one (out of nine) H-ATLAS sources with flux densities at 350 μm $\simeq$ 300 mJy and $z \geq 1$, over the entire H-ATLAS phase 1 area, is associated with a *Planck* detection. Indeed, background fluctuations of the order of ≥ 2 sigma are needed to make those sources detectable by *Planck*. The probability of such an event is so extremely low (just a few per cent for Gaussian fluctuations) that even a single occurrence can be considered a stroke of luck. Since the fluctuations are dominated by confusion and have a strong super-Gaussian tail, the frequency of these fluctuations is substantially higher than expected from Gaussian statistics. However, the probability that this fluctuation happens to be by chance on top of a strongly lensed galaxy is tiny (but hard to quantify without knowing the statistics of fluctuations). Therefore the most likely scenario is the one in which H-ATLAS J114637.9-001132 is associated with a clump of sources, most of which fall below the H-ATLAS detection limit, but their total integrated flux is seen as a positive fluctuation by *Planck*, due to its relatively large beam.

Figure 12 shows the distribution of F_{545}/F_{353} vs. F_{857}/F_{545} colours for the ERCSC sources in the H-ATLAS fields (black, orange, and big red dots) and the rest of ERCSC sources with $|b| > 20^\circ$ and with 3σ detections or better (small purple dots), compared to model SED colour tracks for two star-forming and one normal spiral galaxy templates going from $z = 0$ to $z = 4.5$ with a $z = 0.5$ interval. The black dots correspond to the sources we have classified as Galactic cirrus, whereas orange dots denote sources that are thought to be truly extragalactic. The red dot corresponds to G12H29. Its isolated position in the diagram suggests that there will be very few other objects like this in the ERCSC[5]. However, the large photometric errors in Fig. 12 make it hard to extract strong statements from it.

6. Conclusions

A cross-correlation of the *Planck* ERCSC with the catalogue of *Herschel*-ATLAS sources detected in the phase 1 fields, covering 134.55 deg^2, has highlighted several problems that need to be solved to correctly interpret the data from the *Planck* sub-mm surveys.

- Contamination by diffuse Galactic emission is a serious problem, as demonstrated by the fact that even in a region of moderate Galactic emission (GAMA-09) all 857 GHz ERCSC sources seem to be associated with cirrus. Therefore, to estimate e.g. the number counts of extragalactic sources, it is crucial to carefully select regions of low Galactic emission. A cirrus flag ≥ 0.125 and the "extended" flag, as defined in Planck Collaboration (2011b), are remarkably effective in picking up probable cirrus, but are not 100% reliable.
- We find a good, essentially linear, correlation between ERCSC flux densities at 857 GHz and SPIRE flux densities at 350 μm above $S_{\rm ERCSC} \simeq 1.5$ Jy. We also find a good correlation between ERCSC flux densities at 545 GHz for sources $S_{\rm ERCSC} \geq 1$ Jy and SPIRE flux densities at 500 μm, after a colour correction has been applied to SPIRE flux densities to take into account the different central wavelengths of the bands. Excluding the large edge-on disk galaxy NGC 5746, whose H-ATLAS flux density is different form the ERCSC values probably due to resolution and background subtraction systematic effects, we find $\langle S_{\rm H-ATLAS} - S_{\rm ERCSC} \rangle \simeq 0.1$ Jy at 857 GHz and $\langle S^*_{\rm H-ATLAS} - S_{\rm ERCSC} \rangle = -0.16$ Jy at 545 GHz. ERCSC flux densities are affected by flux boosting and have $\geq 30\%$ uncertainties below ~ 1.3 Jy. The relative difference between *Herschel* and *Planck* flux densities is compatible with these error levels and the calibration uncertainties of both experiments. The mean difference between ERCSC and H-ATLAS positions for 857 GHz sources brighter than 1.5 Jy is 0.42 arcmin, with a dispersion of 0.17 arcmin, confirming the accuracy of ERCSC positions.
- In addition to the contamination from Galactic thermal dust emission, the *Planck* sub-mm surveys are limited by confusion from faint sources within the beam, as expected (e.g. Negrello et al. 2004; Fernandez-Conde et al. 2008). A significant contribution to confusion fluctuations is clustering (Planck Collaboration 2011c). Occasionally, the confusion fluctuations may be dominated by a single protocluster of star-forming galaxies (Negrello et al. 2005). Alternatively, the confusion fluctuations may be caused by apparent clustering due to a random alignment of galaxies at different redshifts. We presented evidence suggesting that at least one object with an anomalous contamination from confusion fluctuations has been detected within the H-ATLAS phase 1 fields. This source is a mixture of a strongly lensed galaxy

[5] Another interesting feature of this diagram, somewhat beyond the focus of this paper, are the eight isolated purple dots that appear in the lower left part of the plot: seven of them correspond to blazars identified in the ERCSC (López-Caniego et al. 2012).

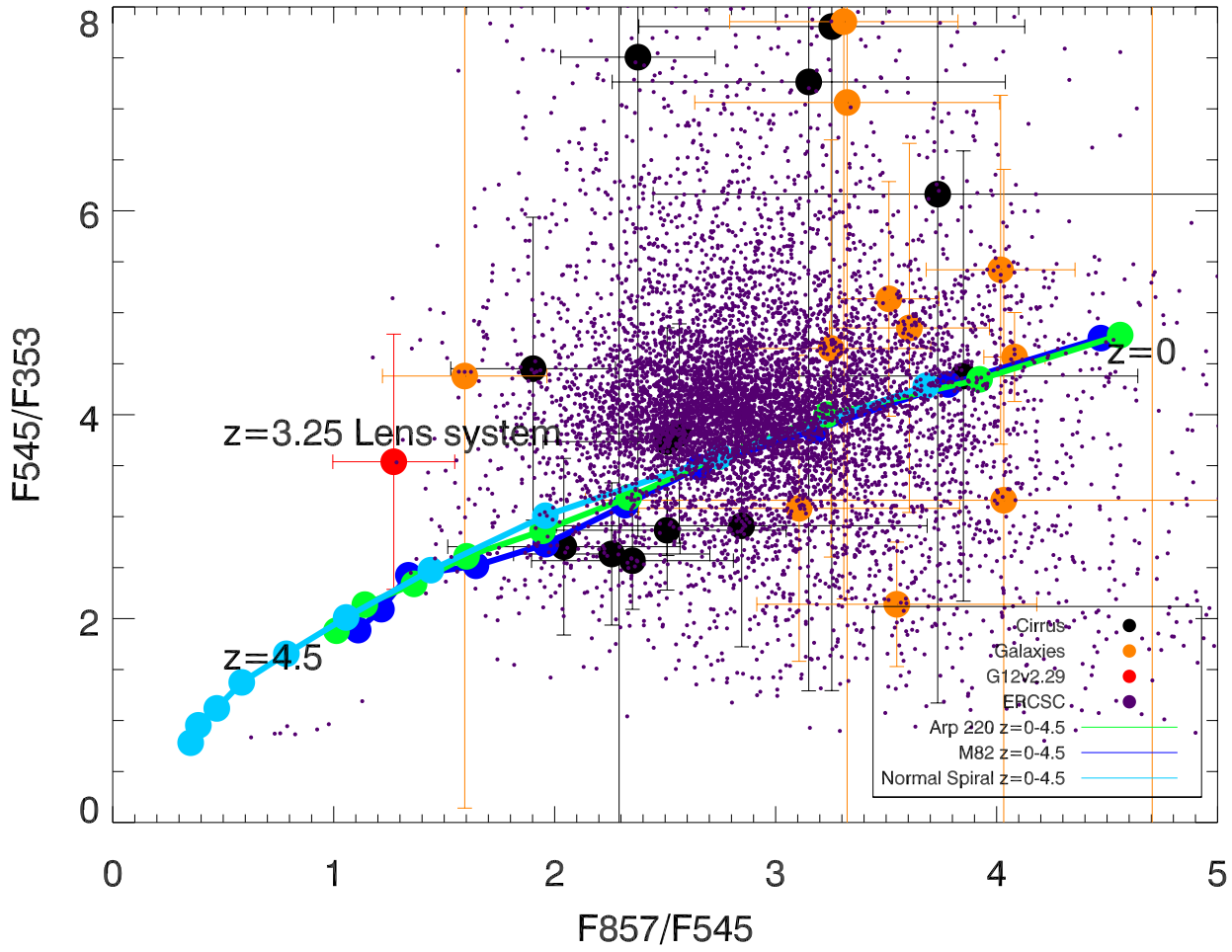

Fig. 12. *Planck* colours of detected objects in the H-ATLAS phase 1 regions compared to model SED colour tracks for two star-forming and one normal spiral galaxy template. The template SEDs go from $z = 0$ to $z = 4.5$, with the dots along the lines spaced by $\Delta z = 0.5$. The large dots show the ERCSC sources within the H-ATLAS fields; the 1 sigma error bars for these sources are also included in the plot. A colour code has been assigned based on our classification using the *Herschel* images: orange dots correspond to sources we classify as galaxies, whereas black dots are classified as Galactic cirrus. H-ATLAS J114637.9-001132 (alias G12H29) is shown in red. For comparison, all ERCSC sources with $|b| > 20°$ and with 3σ detections or better are also shown as purple points. Seven of the eight isolated purple points in the lower left corner of the plot correspond to blazars identified in the ERCSC (López-Caniego et al. 2012).

at $z = 3.26$ surrounded by a statistically significant overdensity of faint galaxies detected by SPIRE. This unusual overdensity of faint galaxies plus an excess of confusion fluctuations at the same position has made it possible for the ERCSC to detect a high-redshift lensed galaxy that would otherwise be below the *Planck* detection limit. The available information is insufficient to reliably estimate the redshift of the galaxies in this clump, although there are some indications that at least the lensing galaxies are at $z \sim 1$. Upcoming PACS photometry and near-IR follow-up of the galaxies in this clump will allow us to better constrain the photometric redshifts of its galaxies. If the rest of the galaxies of the clump could be shown to be at the same redshift, this would represent an example showing the power of combining *Planck* and *Herschel* data. Such a combination may open a new window for the study of cluster evolution, since the main searches carried out so far at similar redshifts have selection functions that are different to that of sub-mm surveys. X-ray and Sunyaev-Zel'dovich (SZ) effect surveys preferentially find massive and evolved structures, dominated by passive early type galaxies; the body of work on SZ-detected clusters is growing quickly (Planck Collaboration 2011d, 2012; Williamson et al. 2011; Story et al. 2011; Stanford et al. 2012; Stalder et al. 2012) and maybe in a near future a number of objects similar to those discussed here will be directly observed. Optical/nearIR cluster-finding algorithms, depending on what detection technique is used, can be biased to red evolved galaxies (e.g. red sequence fitting) but this is not always the case (van Breukelen et al. 2006). The sub-mm selection could find clusters with a high level of star-formation activity, thus shedding light on this poorly known phase of their evolution (Michałowski et al. 2010).

– Although our statistics are too poor to reach definite conclusions, simple source-blending seems to be a less frequent problem: in only one case has an ERCSC 857 GHz source been resolved by *Herschel* into two similarly bright objects, and in general, the contribution of lower luminosity H-ATLAS sources to the flux density measured by *Planck* was minor (see Fig. 8).

In conclusion, we find that the higher sensitivity and higher angular resolution H-ATLAS maps provide key information for

the interpretation of candidate sources extracted from *Planck* sub-mm maps. The phase 1 survey considered in this paper represents ∼1/4 of the full H-ATLAS (550 deg^2). Therefore, the results presented here will be substantially improved once the H-ATLAS survey is completed.

Of special interest is the possibility that *Planck* may be able to sample the tail of the distribution of high-z over-densities, providing unique information about both the early evolution of large-scale structure and galaxy formation and evolution in high-density environments.

Acknowledgements. The *Herschel*-ATLAS is a project with *Herschel*, which is an ESA space observatory with science instruments provided by European-led Principal Investigator consortia and with important participation from NASA. The H-ATLAS website is http://www.h-atlas.org/. D.H. and M.L.C. acknowledge partial financial support from the Spanish Ministerio de Ciencia e Innovación project AYA2010-21766-C03-01 and the Consolider Ingenio-2010 Programme project CSD2010-00064. D.H. also acknowledges the Spanish Ministerio de Educación for a José Castillejo' mobility grant with reference JC2010-0096 and the Astronomy Department at the Cavendish Laboratory for their hospitality during the elaboration of this paper. The Italian group has been supported in part by ASI/INAF agreement No. I/009/10/0 and by INAF through the PRIN 2009 "New light on the early Universe with sub-mm spectroscopy". F.J.C. acknowledges partial financial support from the Spanish Ministerio de Ciencia e Innovación project AYA2010-21490-C02-01.

References

Aatrokoski, J., Ade, P. A. R., Aghanim, N., et al. 2011, Explanatory Supplement to the Planck Early Release Compact Source Catalogue, Tech. rep., ESA
Abazajian, K. N., Adelman-McCarthy, J. K., Agüeros, M. A., et al. 2009, ApJS, 182, 543
Bracco, A., Cooray, A., Veneziani, M., et al. 2011, MNRAS, 412, 1151
Brammer, G. B., van Dokkum, P. G., & Coppi, P. 2008, ApJ, 686, 1503
Cox, P., Krips, M., Neri, R., et al. 2011, ApJ, 740, 63
Dale, D. A., Aniano, G., Engelbracht, C. W., et al. 2012, ApJ, 745, 95
Eales, S., Dunne, L., Clements, D., et al. 2010, PASP, 122, 499
Fernandez-Conde, N., Lagache, G., Puget, J.-L., & Dole, H. 2008, A&A, 481, 885
Fu, H., Jullo, E., Cooray, A., et al. 2012, ApJ, 753, 134
González-Nuevo, J., Lapi, A., Fleuren, S., et al. 2012, ApJ, 749, 65
Griffin, M. J., Abergel, A., Abreu, A., et al. 2010, A&A, 518, L3
Harris, A. I., Baker, A. J., Frayer, D. T., et al. 2012, ApJ, 752, 152
Ivison, R. J., Swinbank, A. M., Swinyard, B., et al. 2010, A&A, 518, L35
Karachentsev, I. D., Pronik, V. I., & Chuvaev, K. K. 1976, A&A, 51, 185
Lapi, A., Gonzalez-Nuevo, J., Fan, L., et al. 2011, ApJ, 742, 24
López-Caniego, M., González-Nuevo, J., Massardi, M., et al. 2012, MNRAS, submitted [arXiv:1205.1929]
Michałowski, M., Hjorth, J., & Watson, D. 2010, A&A, 514, A67
Miville-Deschênes, M.-A., & Lagache, G. 2005, ApJS, 157, 302
Negrello, M., Magliocchetti, M., Moscardini, L., et al. 2004, MNRAS, 352, 493
Negrello, M., González-Nuevo, J., Magliocchetti, M., et al. 2005, MNRAS, 358, 869
Negrello, M., Hopwood, R., De Zotti, G., et al. 2010, Science, 330, 800
Pilbratt, G. L., Riedinger, J. R., Passvogel, T., et al. 2010, A&A, 518, L1
Planck Collaboration 2006, The Scientific Programme of Planck [arXiV:astro-ph/0604069]
Planck Collaboration 2011, VizieR Online Data Catalog, 8088, 0
Planck Collaboration 2011a, A&A, 536, A1
Planck Collaboration 2011b, A&A, 536, A7
Planck Collaboration 2011c, A&A, 536, A18
Planck Collaboration 2011d, A&A, 536, A8
Planck Collaboration 2012, A&A, 543, A102
Planck HFI Core Team 2011, A&A, 536, A6
Poglitsch, A., Waelkens, C., Geis, N., et al. 2010, A&A, 518, L2
Rieke, G. H., Young, E. T., Engelbracht, C. W., et al. 2004, ApJS, 154, 25
Rigby, E. E., Maddox, S. J., Dunne, L., et al. 2011, MNRAS, 415, 2336
Serjeant, S., & Harrison, D. 2005, MNRAS, 356, 192
SPIRE Observers' Manual v2.2 2010, Herschel Science Centre, HERSCHEL-DOC-0798
Stalder, B., Ruel, J., Suhada, R., et al. 2012, ApJ, submitted [arXiv:1205.6478]
Stanford, S. A., Brodwin, M., Gonzalez, A. H., et al. 2012, ApJ, 753, 164
Story, K., Aird, K. A., Andersson, K., et al. 2011, ApJ, 735, L36
Swinbank, A. M., Smail, I., Longmore, S., et al. 2010, Nature, 464, 733
Tauber, J. A., Mandolesi, N., Puget, J., et al. 2010, A&A, 520, A1
van Breukelen, C., Clewley, L., Bonfield, D. G., et al. 2006, MNRAS, 373, L26
Wall, J., & Jenkins, C. 2003, Practical Statistics for Astronomers, Cambridge Observing Handbooks for Research Astronomers (Cambridge University Press)
Williamson, R., Benson, B. A., High, F. W., et al. 2011, ApJ, 738, 139
Zacchei, A., Maino, D., Baccigalupi, C., et al. 2011, A&A, 536, A5